

# Transmission of xenon scintillation light through PTFE

---

D. Cichon,<sup>a,1</sup> G. Eurin,<sup>a,2</sup> F. Jörg,<sup>a,1</sup> T. Marrodán Undagoitia,<sup>a</sup> N. Rupp<sup>a</sup>

<sup>a</sup>Max-Planck-Institut für Kernphysik, Saupfercheckweg 1, 69117 Heidelberg, Germany

E-mail: [dominick.cichon@mpi-hd.mpg.de](mailto:dominick.cichon@mpi-hd.mpg.de), [florian.joerg@mpi-hd.mpg.de](mailto:florian.joerg@mpi-hd.mpg.de)

**ABSTRACT:** Polytetrafluoroethylene (PTFE), also known as Teflon, is a common material used in the construction of liquid xenon detectors due to its high reflectivity for the VUV scintillation light of xenon. We present measurements of the transmittance of PTFE for xenon scintillation light with peak emission at a wavelength of 175 nm. PTFE discs of different thicknesses are installed in front of a photosensor in two setups. One is filled with gaseous xenon, the other with liquid xenon. The measurements performed with the gaseous xenon setup at room temperature yield a transmission coefficient of  $\lambda_t = (350^{+60}_{-0} \text{ (sys)} \pm 50 \text{ (stat)}) \mu\text{m}$ . This is found to be in agreement with the observations made using the liquid xenon setup.

**KEYWORDS:** Noble liquid detectors, detector design and construction technologies and materials, dark matter detectors, double beta decay detectors

---

<sup>1</sup>corresponding author

<sup>2</sup>now at CEA/Saclay, IRFU (Institut de Recherche sur les Lois Fondamentales de l'Univers), F-91191 Gif-sur-Yvette CEDEX, France

---

## Contents

<b>1</b>	<b>Introduction</b>	<b>1</b>
<b>2</b>	<b>Detector setups</b>	<b>2</b>
<b>3</b>	<b>Data analysis</b>	<b>4</b>
<b>4</b>	<b>Results and discussion</b>	<b>7</b>
<b>5</b>	<b>Conclusion</b>	<b>9</b>

---

## 1 Introduction

In the search for rare processes, such as the elastic scattering of particle dark matter off nuclei [1] or the search for neutrinoless double beta decay [2], liquid xenon detectors have shown great performance and excellent sensitivity [3–6]. These detectors reconstruct the energy deposited by particles using xenon scintillation signals. Such signals are typically detected with photosensors sensitive to vacuum ultraviolet (VUV) light. The scintillation wavelength of xenon is centered in the vacuum ultraviolet regime at  $(174.8 \pm 0.1 \text{ (stat.)} \pm 0.1 \text{ (syst.)})$  nm as pointed in recent spectroscopic measurements [7] (in contrast to previous measurements that reported the peak emission closer to 178 nm [8, 9]). In order to efficiently collect the emitted photons in a detector, VUV reflectors are required. Current liquid xenon (LXe) detectors employ polytetrafluoroethylene (PTFE, also known as Teflon) for this purpose [10–13] due to its excellent reflectivity properties. The reflectivity of PTFE is measured to be between 37% and 100% depending on the surface finishing and the surrounding medium [14–17]. While measurements in vacuum [15] or argon atmosphere [14] point to lower reflectivity values, the ones in LXe (direct measurements or extracted from MC/data comparisons) are close to 100% [15–17].

The reduction of experimental backgrounds is a major enterprise in experiments searching for rare processes. Radioactive trace impurities, such as uranium and thorium, are commonly found in most detector materials [18]. Their subsequent  $\alpha$ -decays can cause the production of radiogenic neutrons via  $(\alpha, n)$  reactions. They can pose a dangerous background for dark matter searches as they produce nuclear recoil signals identical to the ones expected by dark matter interactions [1]. Since the cross-section for  $(\alpha, n)$  reactions on fluorine is high [19], the overall amount of PTFE needs to be minimized. This would potentially also reduce background from other radionuclides, such as  $\gamma$ -radiation originating from the decay of  $^{214}\text{Bi}$ , which is a limiting factor for neutrinoless double beta decay searches [20]. However, if a too thin sheet is employed, transmission of light through the PTFE could become significant, leading to signal losses. Furthermore, experiments using an outer veto detector, for example XENON100 [21] or LZ (in construction) [11], could suffer from light leaking into the veto region, making data analysis significantly more complex. We report here on a study of the transmittance of PTFE for xenon scintillation light.

## 2 Detector setups

Two setups are employed to measure the transmittance of PTFE for xenon scintillation light. Most of the measurements were performed in a small chamber at room temperature filled with gaseous xenon (GXe). To check the behavior in LXe, additional tests were subsequently performed using a LXe time projection chamber (TPC).

Figure 1 shows a schematic of the used room temperature setup. It consists of a 47 cm long

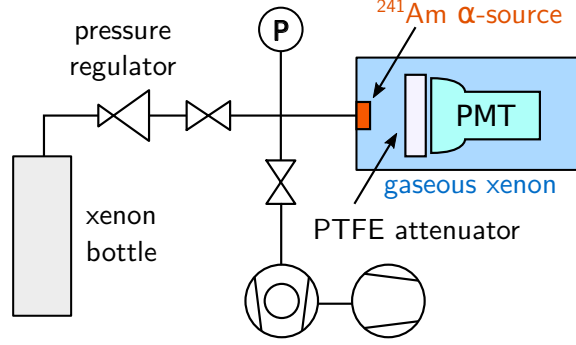


**Figure 1.** Schematic of the room temperature setup.

stainless steel tube into which a structure holding both a photomultiplier tube (PMT) and a PTFE disc is inserted. The tube is filled with GXe at an average pressure of  $(1098 \pm 7)$  mbar. An  $^{241}\text{Am}$   $\alpha$ -source ( $Q_\alpha = 5.6$  MeV), mounted on the tube backplate, is used to produce scintillation light in the xenon gas. Since the scintillation spectra of GXe and LXe are very similar [8], this setup is expected to be a valid approximation. The distance between the  $^{241}\text{Am}$  source and the PTFE disc is fixed to  $(14.0 \pm 0.3)$  cm using three threaded rods. Scintillation photons are detected via a 3 inch Hamamatsu R11410-21 PMT [22]. Its signal is recorded via a CAEN V1724 digitizer triggered by an external discriminator. The PMT's gain has been measured at several voltages during the testing campaign described in [22].

PTFE discs in 6 different thicknesses, called attenuators from now on, were tested individually by placing them directly in front of the PMT window in order to measure the amount of scintillation light passing through. All discs were manufactured from the same raw material of extruded, natural PTFE [23], where half of them were made using a lathe with a backplate for supporting the material (batch 1). The other half was produced with a mill which utilized vacuum suction for material support (batch 2). The attenuator thicknesses were determined using a Mitutoyo ID-F150 digital dial gauge. Each attenuator was measured at 49 points distributed uniformly in  $(r^2, \varphi)$  over the area covering the PMT window. The results can be found in Table 1. Attenuators belonging to the second batch show, on average, a more homogeneous thickness across their surface than the ones produced in the first batch. This can be explained by a better sample support due to the vacuum table during the production of batch 2. In addition, a measurement without attenuator was performed.

After each measurement, the setup needs to be opened to exchange the attenuator. Since impurities from the air, such as water, could cause additional attenuation of the scintillation light due to absorption [24], the opening is performed inside a gas-tight bag continuously flushed with nitrogen. To guarantee equivalent conditions among the different measurements, special attention

**Table 1.** List of the PTFE attenuators used in the GXe setup. Values given for the thickness and its error are taken from the mean and the standard deviation of the 49 measurements made for each attenuator, respectively.

attenuator	thickness [ $\mu\text{m}$ ]	production batch
1	$97 \pm 2$	2
2	$283 \pm 4$	2
3	$442 \pm 6$	1
4	$737.6 \pm 1.3$	2
5	$965 \pm 4$	1
6	$1310 \pm 30$	1

was paid to the outgassing of the PTFE attenuators themselves. All of them were cleaned by applying a detergent and rinsing them three times using de-ionized water. Afterwards, the samples were submerged in ethanol and put into a drying chamber through which a continuous flow of 200 SCCM nitrogen at a pressure of 50 mbar is maintained. Exchange of each sample was done following a timed schedule, such that setup opening, evacuation, and xenon filling durations as well as the time between data taking and evacuation start were kept the same. The maximum deviation from this schedule during the measurement campaign is estimated to be smaller than 2 min.

The results of the measurement described above are cross-checked with measurements using a local LXe TPC, Heidelberg Xenon (HeXe) [25, 26], illustrated in Figure 2.

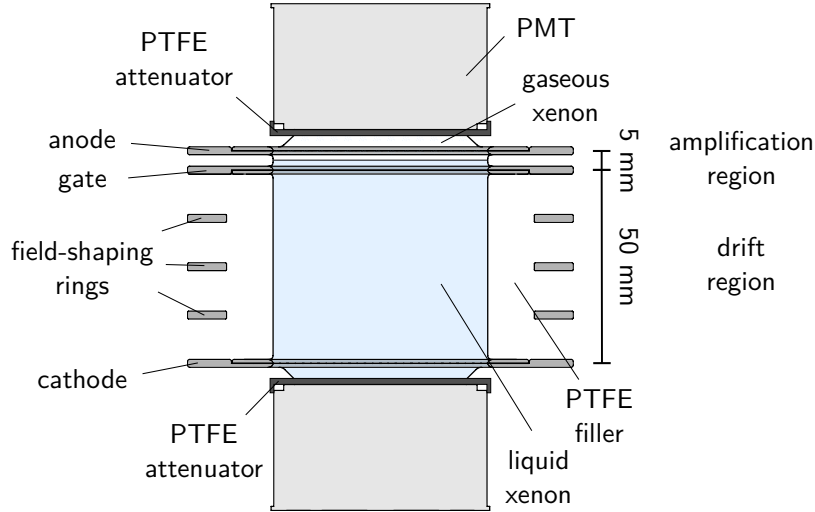


**Figure 2.** Simplified diagram of the HeXe TPC which is encased in PTFE. Attenuators are colored in black here for easier visibility.

It contains a cylindrical sensitive volume of 5.6 cm diameter and 5 cm height enclosed by PTFE. Electric fields are generated by three electrodes having a hexagonal meshed structure — anode, gate, and cathode — together with three field-shaping rings, all of them made out of stainless steel. Cathode, field-shaping rings and gate are connected in series via 1 G $\Omega$  resistors and define a homogenous drift field by applying a voltage between cathode and gate, while a voltage applied between gate and anode creates the extraction field. To detect the scintillation light, two 2 inch

Hamamatsu R6041-406 PMTs are placed at the top and bottom of the sensitive volume, respectively. They are periodically calibrated *in situ* following the technique described in [27].

For the measurements presented here, data from  $^{83m}\text{Kr}$  and  $^{222}\text{Rn}$  decays inside the TPC were acquired.  $^{222}\text{Rn}$  is extracted from an aqueous  $^{226}\text{Ra}$  solution by freezing it into an active charcoal trap, while  $^{83m}\text{Kr}$  is continuously emanated from  $^{83}\text{Rb}$ -containing zeolite beads [28, 29] inside a stainless steel tube. Both unstable nuclides can individually be mixed into the xenon via a gas purification system, by directing the gas flow through either of the two sources.  $\alpha$ -decays from the  $^{222}\text{Rn}$  decay chain cannot be accurately measured in HeXe due to their scintillation signals saturating the PMTs. To prevent this saturation, light attenuators made from PTFE were installed. The measurements in gaseous xenon at room temperature presented here were carried out to find the PTFE attenuator thickness best suited for measuring  $\alpha$ -decays with HeXe in liquid xenon.

The attenuators were wiped with ethanol in an  $\text{N}_2$  atmosphere and inserted into the TPC following the same opening procedure as in [30].

### 3 Data analysis

#### 3.1 Room temperature measurements

In the room temperature setup, the amount of scintillation light transmitted through the PTFE discs is determined by finding and integrating over the PMT signals using the same data processor as described in [25]. Figure 3 shows the part of the scintillation spectrum corresponding to the full absorption of the  $^{241}\text{Am}$   $\alpha$ -particle for each attenuator (normalized to the peak maximum). The peak's shape is found to be well described by a two-sided Gaussian function of the form:

$$f(x) = N \cdot \begin{cases} e^{-\frac{1}{2}\left(\frac{x-\mu}{\sigma_1}\right)^2} & x < \mu \\ e^{-\frac{1}{2}\left(\frac{x-\mu}{\sigma_2}\right)^2} & x \geq \mu \end{cases} \quad (3.1)$$

Here,  $\mu$  represents the central peak position, with the  $\sigma_i$  representing the peak widths left and right to the central position respectively and  $N$  being a scale factor. After a preliminary manual fit for extracting initial values for the widths ( $\sigma'_i$ ), the range of the final fit is constrained to  $[\mu - 2\sigma'_1, \mu + 2\sigma'_2]$  as indicated by the solid lines in Figure 3. Dashed lines show the continuation of the functions outside of the fitted range and indicate reasonable agreement of the data with the fit. In all measured spectra, the peak is well above the cutoff caused by the threshold of the external discriminator used for triggering the acquisition of data.

In addition to the full absorption peaks shown in Figure 3, each spectrum exhibits two additional features. At twice the average signal size of each full absorption peak, an additional peak is observed which corresponds to two  $\alpha$ -decay signals from pile-up. This has been confirmed on signal waveforms. Another peak, located at  $< 25\%$  of the full absorption peak mean, can be explained by  $\alpha$ -particles stopped by the top ring of the source holder. This can happen in cases when a particle is emitted under a shallow angle relative to the source surface. As a consequence, they deposit only a fraction of their energy in the xenon gas, leading to a reduction of scintillation light. This hypothesis is qualitatively confirmed by using a Monte Carlo simulation to determine

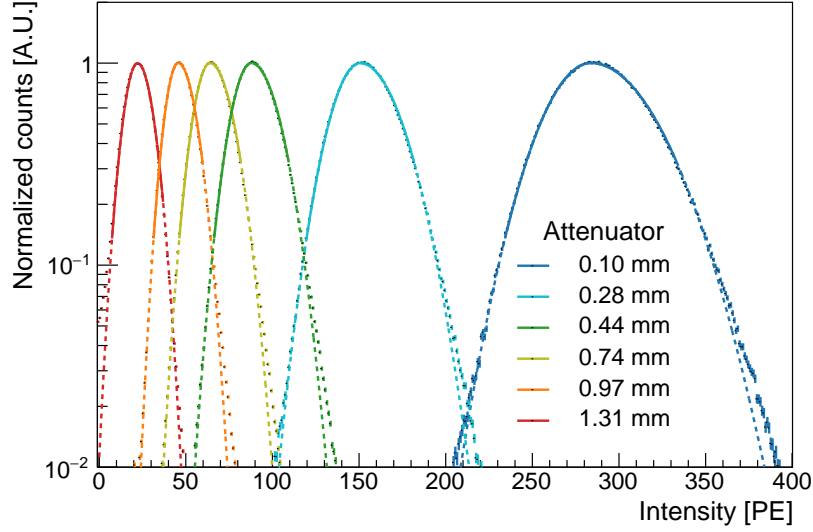


**Figure 3.** Full absorption peaks of  $^{241}\text{Am}$   $\alpha$ -decays measured in the room temperature setup. Spectra were normalized to their respective peak height. A two-sided Gaussian function is fitted to each peak, with the fit range indicated by the solid lines.

the track length distribution for particles which are stopped by the source holder and comparing it to the range in GXe (determined to be 21 mm on average using SRIM [31]), assuming the amount of light to be proportional to the track length. Event pile-up between these clipped tracks and full absorption events, as well as different light collection efficiencies depending on the  $\alpha$ -particle direction, could be possible reasons for the asymmetric shape of the full absorption peak.

Besides the statistical errors from the fit, systematic errors affecting the average signal size are also taken into account. The most relevant one is due to variations in the distance between the  $^{241}\text{Am}$  source and the PTFE attenuator of up to 3 mm in either direction. The related uncertainty was estimated using an optical simulation and amounts to 4%. Another contribution (0.7%) comes from an observed linear decrease in light yield during each measurement, likely caused by emanation of impurities into the xenon as soon as it is filled into the setup. Although the decrease is corrected for, the remaining error comes from possible variations of the measurement schedule which result in the time between data acquisition and setup filling to differ up to  $\Delta t = 1\text{ min}$ . Furthermore, potential variation of the PMT's gain between measurements could introduce an additional uncertainty of 0.6%, as its operating voltage could only be set with an accuracy of  $\Delta V = 1\text{ V}$ . Finally, the impact of the fit range choice is also accounted for by varying the fit interval endpoints between  $\pm 1\sigma \dots \pm 3\sigma$  (up to 1.5%). While the pressure of the filled xenon gas varied up to 0.6%, the impact on the light yield is assumed to be negligible [32].

### 3.2 HeXe measurements

To assess the PTFE transmittance in LXe, two sets of attenuators were inserted into the TPC described in Section 2. Their respective thicknesses and positions within the detector are summarized

in Table 2. Given the inhomogeneous thickness introduced by a hole drilled into the 3.3 mm thick disc covering the top PMT in the second measurement, this attenuator is not taken into account for further comparisons.

**Table 2.** PTFE attenuators used in the HeXe setup for comparison of their attenuation in LXe.

attenuator	measurement	PMT	phase	thickness
1	a	top	GXe	175 $\mu\text{m}$
2		bottom	LXe	550 $\mu\text{m}$
3	b	top	GXe	3.3 mm *
4		bottom	LXe	700 $\mu\text{m}$

\* Attenuator with inhomogeneous thickness due to a hole.

Energy depositions in the TPC's sensitive volume by  $\alpha$ -decays of  $^{222}\text{Rn}$  and its daughters  $^{218}\text{Po}$  and  $^{214}\text{Po}$  were recorded during dual-phase operation. The average amount of light seen by each photosensor is then determined by first selecting decays which happened within  $\pm 1$  mm around the central height of the TPC. Then, the amount of prompt scintillation light seen by the top PMT is plotted against the amount seen by the bottom one. Finally, a 2D Gaussian function is fitted to the population corresponding to the  $\alpha$ -decays of  $^{222}\text{Rn}$  and  $^{218}\text{Po}$  (see Figure 4). These decays are grouped together as their expected full absorption peaks cannot be resolved separately.

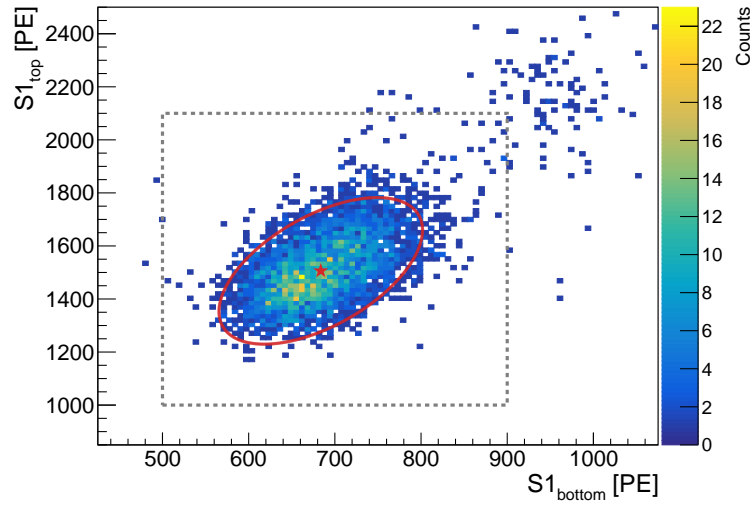


**Figure 4.** Detected signal size in the top and the bottom PMTs of the HeXe setup.  $\alpha$ -decays of  $^{222}\text{Rn}$  and its decay products happening in the central 2 mm of the TPC height are shown. A bivariate Gaussian function (red contour) is fitted to the data falling into the gray box. Its mean is highlighted by the red star. Data corresponds to *measurement a* (see Table 2).

To compare the average amount of light seen in HeXe with the room temperature setup data, the expected amount of light for  $^{222}\text{Rn}$  (daughter)  $\alpha$ -decays in HeXe without attenuators needs to

be estimated. As such measurements suffer from signal loss due to PMT saturation effects, this quantity can only be determined indirectly. Therefore, the signal size of  $^{83m}\text{Kr}$  decays as recorded by the top/bottom PMT in the HeXe setup without attenuators ( $LY^{\text{HeXe}}(\text{Kr})_{t,b}$ ), is multiplied with the signal size ratio between  $^{222}\text{Rn}$  and  $^{83m}\text{Kr}$  signals as observed in XENON100<sup>1</sup> [33, 34]. In the latter, PMT saturation effects when recording  $\alpha$ -decays were significantly less pronounced and could be corrected for. Decays of  $^{83m}\text{Kr}$  cannot be used to compare light levels with and without attenuator on their own, as they generate too little light which makes them non-detectable when the attenuators mentioned in Table 2 are present. In addition, the signal needs to be corrected for the modified probability for a photon to reach the top or the bottom PMT due to reflection off the PTFE attenuators. This is necessary to disentangle the effects of both reflection and absorption on the photon detection efficiency. The correction is applied by multiplying the amount of light seen by each PMT with a factor which depends on the probability for a photon to hit the PMT if no absorption were to take place in either attenuator (called  $P$  from now on). An optical GEANT4 [35] simulation of the HeXe setup was used to study how the presence of PTFE attenuators modifies  $P$ . Absorption inside the simulated PTFE attenuators was disabled. The correction factor is given as the ratio between  $P(\text{no attenuators})$  and  $P(\text{with attenuators})$ . The attenuation factor  $\gamma_i$  for the PTFE piece in front of PMT  $i = \{t, b\}$  can then be calculated using the following equation:

$$\gamma_i = \left[ \frac{LY^{\text{HeXe}}(\text{Rn})}{LY^{\text{HeXe}}(\text{Kr})} \right]_{i=\{t,b\}} \cdot \left[ \frac{P(\text{no attenuators})}{P(\text{with attenuators})} \right]_{i=\{t,b\}} \cdot \frac{LY^{\text{XE100}}(\text{Kr})}{LY^{\text{XE100}}(\text{Rn})}. \quad (3.2)$$

Because no dedicated reflectivity measurements of the PTFE pieces could be made, a range of potential values taken from attenuation measurement data and literature has to be taken into account. Reflectivity of PTFE in the GXe phase is assumed to be 76% based on room temperature setup data (explained in Section 4). For PTFE without a dedicated surface finishing, a reflectivity of 96% is assumed when immersed in LXe, similar to values reported for example by [17]. To quantify the uncertainty due to the range of potential reflectivities, the assumed values are varied by  $\pm 30\%$ , covering the range of typical literature values for the reflectivity of PTFE [14, 17]. This yields an estimate for the relative systematic uncertainty of about 50%. The impact of variations in the liquid level height as well as the reflectivity of the stainless steel meshes was investigated as well, but found to be subdominant.

## 4 Results and discussion

The observed average  $\alpha$ -decay signal size is calculated as described in Sections 3.1 and 3.2 as a function of the thickness of the PTFE attenuator used for the corresponding measurement. Figure 5 shows the data of the room temperature setup in purple, while the measurements in the HeXe setup are shown in orange and green for attenuators placed in the gas and liquid xenon phase, respectively.

Assuming the Beer-Lambert law to be applicable, the amount of light  $I$  transmitted through a PTFE attenuator of thickness  $d$  is modelled by:

$$I(d) = A \cdot e^{-\frac{d}{\lambda_t}} + B, \quad (4.1)$$

---

<sup>1</sup> $LY^{\text{XE100}}(\text{Kr})/LY^{\text{XE100}}(\text{Rn}) = 173 \pm 4$

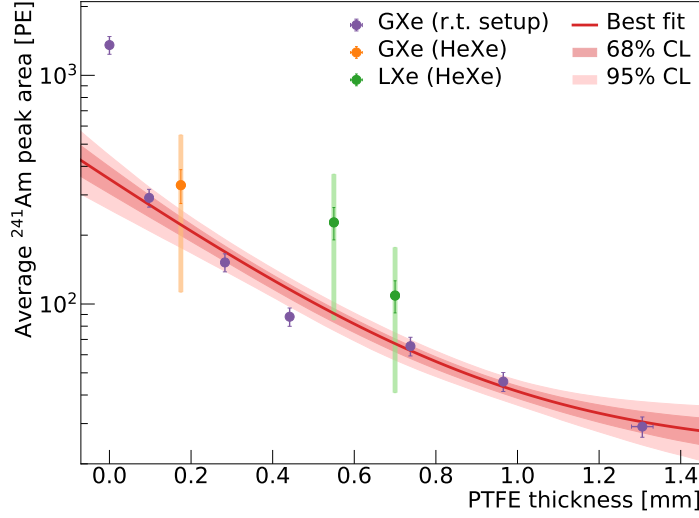


**Figure 5.** Average  $\alpha$ -decay xenon scintillation signal size in photo electrons (PE) versus PTFE attenuator thickness. The data acquired at room temperature (purple markers) are fitted with a modified Beer-Lambert function (equation 4.1), where the red shaded regions are the respective confidence bands of the fit function. For data points inferred using the HeXe setup, statistical uncertainties are shown separately from the combined error. The contribution of the former is indicated with vertical bars in the same color as the data point, while the combination of both the statistical uncertainty and systematic uncertainties from the optical simulation is shown using a brighter shade.

where  $A$  denotes the amount of transmitted light expected for an infinitesimally thin attenuator and  $\lambda_t$  represents the effective transmission coefficient of the medium. The constant offset  $B$  allows for scattered light bypassing the attenuator to be taken into account which is found to be necessary to explain the data. Equation 4.1 is fitted to the room temperature data (purple points, excluding the data point taken without attenuator) by minimizing  $\chi^2$  in order to extract the transmission coefficient, giving

$$\lambda_t = (350^{+60}_{-0} \text{ (sys)} \pm 50 \text{ (stat)}) \mu\text{m},$$

Here the statistical uncertainty of  $\pm 50 \mu\text{m}$  is determined from the fit, taking into account variations of the PTFE thickness, as well as the uncertainties on the light level which are detailed in Section 3.1. The constant  $B$  is found to be  $(23 \pm 6)$  PE.

The data point obtained without attenuator deviates from the value expected by extrapolation of the fit result, which is given by parameter  $A$  in Equation 4.1 and amounts to  $(330 \pm 50)$  PE. We explain this deviation by the Fresnel reflection at the PTFE surface. For all the measurements with an attenuator, part of the incoming scintillation light is lost due to reflection. Using this measurement, a reflectivity of about 76% of the used PTFE in GXe is found.

Since scintillation light is produced isotropically along the track length of the  $\alpha$ -particles, photons do not always arrive perpendicular with respect to the attenuator surface. If scattering of the light inside the PTFE is not taken into account, the amount of PTFE traversed before reaching the

PMT depends on the angle of incidence, resulting in a larger effective thickness of the attenuators. The distribution of incident angles has been determined using an optical GEANT4 simulation of the room temperature setup, assuming isotropic emission of photons within a hemispheric region around the  $^{241}\text{Am}$  source having a radius of 21 mm. The mean traversed PTFE thickness varies for different assumptions made on the reflective properties of the stainless steel tube. To get an estimate for the reflectivity of stainless steel for xenon scintillation light, the measurements reported in [36] were extrapolated to the wavelength of 175 nm. Given the unpolished surface of the tube's steel and that no dedicated surface finishing has been applied, 30 % diffuse reflectivity were assumed. Under this assumption, the average traversed length would then be increased by a factor of 1.16, leading to a 16% larger transmission coefficient. For the highest reported VUV reflectivity of stainless steel (57%) [37] and under the conservative assumption of pure specular reflection, which was found to yield more extreme incident angles than pure diffuse reflection, the effective thickness would be larger by a factor of 1.47 compared to the geometric thickness. Since the exact reflective properties of the used steel are unknown, this effect can not be corrected for. It is therefore reflected by the asymmetric systematic uncertainty of up to +60  $\mu\text{m}$  on the result.

As part of the light is reflected off the PTFE from layers deeper than the surface [38], the total amount of reflected light would depend on the sample thickness. This would cause the transmittance to differ from the one derived from the Beer-Lambert law. Since the used setup does not allow to simultaneously measure the reflectance of the samples, this ambiguity can not be resolved. However, an estimation of the effect due to in-medium scattering on the transmittance was done, using the so-called *two-flux* model originally proposed by Kubelka and Munk [39, 40]. This one dimensional model allows to predict the transmittance through a parallel plane sample. Absorption within the medium is described by an absorption length  $\lambda_a$ , whereas scattering of the light into the forward and backward direction is described by a total effective scattering length  $\lambda_s$ . The transmittances observed in the room temperature setup are found to be well described by this model if a total effective scattering length of  $\lambda_s \sim 50 \mu\text{m}$  together with an absorption length  $\lambda_a \gg \lambda_s$  are assumed. Assuming this model is valid, we find that the predicted transmittance would be greater at larger thicknesses compared to the simple Beer-Lambert-based model which uses  $\lambda_t$  when disregarding the offset  $B$ . The evolution of the transmittance predicted by the two-flux model is compatible with the result reported in [41].

Finally, in order to compare data obtained from both setups with each other, HeXe data points need to be scaled in order to match the light level of the room temperature setup. Consequently, the attenuation factor of each attenuator in the HeXe setup is first determined as described in Section 3.2. It is then applied to the expected  $^{241}\text{Am}$  signal size in the room temperature setup without attenuator, estimated by extrapolation of the fit function to a PTFE thickness of 0 mm. All three data points agree with the fitted line within the combined systematic and  $1\sigma$  statistical error. It should be noted, that the given thicknesses do not include the shrinkage of PTFE at cryogenic temperatures.

## 5 Conclusion

The transmission coefficient of PTFE for xenon scintillation light has been determined for the first time using a setup filled with GXe at room temperature, yielding:

$$\lambda_t = (350^{+60}_{-0} \text{ (sys)} \pm 50 \text{ (stat)}) \mu\text{m}.$$

Complementary measurements with PTFE attenuators inside the HeXe LXe TPC were conducted in addition to verify the result under realistic detector conditions. Their results agree within the statistical and systematic errors with values expected when using the transmission coefficient estimate.

While PTFE is a commonly-used material in LXe detectors due to its high reflectivity for xenon scintillation light, it is desired to reduce its amount to minimize radiogenic background. Knowledge of the transmission of xenon scintillation light thus helps in optimizing the design of future detectors such as DARWIN [42]. The results obtained in this study imply, that PTFE of a few mm thickness is sufficient to optically decouple detector regions from each other.

## Acknowledgments

We wish to acknowledge the support of the the Max Planck Society. We thank our technician Michael Reißfelder for his considerable support regarding both of the experimental setups as well as Lutz Althüser for his comments regarding the effective PTFE thickness.

## References

- [1] T. Marrodán Undagoitia and L. Rauch, *Dark matter direct-detection experiments*, *J. Phys.* **G43** (2016) 013001, [[1509.08767](#)].
- [2] H. Päs, and W. Rodejohann, *Neutrinoless Double Beta Decay*, *New J. Phys.* **17** (2015) 115010, [[1507.00170](#)].
- [3] XENON collaboration, E. Aprile et al., *Dark Matter Search Results from a One Ton-Year Exposure of XENON1T*, *Phys. Rev. Lett.* **121** (2018) 111302, [[1805.12562](#)].
- [4] EXO collaboration, J. B. Albert et al., *Search for Neutrinoless Double-Beta Decay with the Upgraded EXO-200 Detector*, *Phys. Rev. Lett.* **120** (2018) 072701, [[1707.08707](#)].
- [5] LUX collaboration, D. S. Akerib et al., *Results from a Search for Dark Matter in the Complete LUX Exposure*, *Phys. Rev. Lett.* **118** (2017) 021303, [[1608.07648](#)].
- [6] PANDAX-II collaboration, X. Cui et al., *Dark Matter Results from 54-Ton-Day Exposure of PandaX-II Experiment*, *Phys. Rev. Lett.* **119** (2017) 181302, [[1708.06917](#)].
- [7] F. Keiko et al., *High-accuracy measurement of the emission spectrum of liquid xenon in the vacuum ultraviolet region*, *Nucl. Instrum. Meth.* **A795** (2015) 293.
- [8] J. Jortner et al., *Localized Excitations in Condensed Ne, Ar, Kr, and Xe*, *J. Chem. Phys.* **42** (1965) 4250–4253.
- [9] N. Basov et al., *Luminescence of condensed Xe, Kr, Ar and their mixtures in vacuum region of spectrum under excitation by fast electrons*, *J. Lumin.* **1-2** (1970) 834–841.
- [10] XENON collaboration, E. Aprile et al., *The XENON1T Dark Matter Experiment*, *Eur. Phys. J.* **C77** (2017) 881, [[1708.07051](#)].
- [11] LZ collaboration, D. S. Akerib et al., *The LUX-ZEPLIN (LZ) Experiment*, *Nucl. Instrum. Methods Phys. Res. A* **953** (2020) 163047, [[1910.09124](#)].
- [12] PANDAX collaboration, X. Cao et al., *PandaX: A Liquid Xenon Dark Matter Experiment at CJPL*, *Sci. China Phys. Mech. Astron.* **57** (2014) 1476, [[1405.2882](#)].

- [13] M. Auger et al., *The EXO-200 detector, part I: Detector design and construction*, *JINST* **7** (2012) P05010, [[1202.2192](#)].
- [14] C. Silva et al., *Reflectance of Polytetrafluoroethylene (PTFE) for Xenon Scintillation Light*, *J. Appl. Phys.* **107** (2010) 064902, [[0910.1056](#)].
- [15] C. Levy, *Light propagation and reflection off Teflon in liquid xenon detectors for the XENON100 and XENONIT experiments*, PhD Thesis, University of Münster (Germany) (2014) .
- [16] LUX collaboration, D. S. Akerib et al., *Technical Results from the Surface Run of the LUX Dark Matter Experiment*, *Astropart. Phys.* **45** (2013) 34, [[1210.4569](#)].
- [17] F. Neves et al., *Measurement of the absolute reflectance of polytetrafluoroethylene (PTFE) immersed in liquid xenon*, *JINST* **12** (2017) P01017, [[1612.07965](#)].
- [18] XENON collaboration, E. Aprile et al., *Material Radioassay and Selection for the XENONIT Dark Matter Experiment*, *Eur. Phys. J. C* **77** (2017) 890, [[1705.01828](#)].
- [19] R. Heaton et al., *Neutron production from thick-target ( $\alpha$ , n) reactions*, *Nucl. Instrum. Methods Phys. Res. A* **276** (1989) 529 – 538.
- [20] DARWIN collaboration, F. Agostini et al., *Sensitivity of the DARWIN observatory to the neutrinoless double beta decay of  $^{136}\text{Xe}$* , [[2003.13407](#)].
- [21] XENON collaboration, E. Aprile et al., *The XENON100 Dark Matter Experiment*, *Astropart. Phys.* **35** (2012) 573, [[1107.2155](#)].
- [22] P. Barrow et al., *Qualification Tests of the R11410-21 Photomultiplier Tubes for the XENONIT Detector*, *JINST* **12** (2017) P01024, [[1609.01654](#)].
- [23] Auer Kunststofftechnik GmbH & Co. KG, “Material datasheet PTFE.” [http://www.auer-kunststofftechnik.de/pdf/Datenblatt\\_PTFE.PDF](http://www.auer-kunststofftechnik.de/pdf/Datenblatt_PTFE.PDF), accessed 2020-07-16.
- [24] K. Ozone, *Liquid Xenon Scintillation Detector for the New  $\mu \rightarrow e\gamma$  Search Experiment*. PhD thesis, Tokyo U., 2005.
- [25] D. Cichon, *Identifying  $^{222}\text{Rn}$  decay chain events in liquid xenon detectors*, Master’s thesis, University of Heidelberg, 2015.
- [26] F. Jörg, *Investigation of coating-based radon barriers and studies towards their applicability in liquid xenon detectors*, Master’s thesis, University of Heidelberg, 2017.
- [27] R. Saldanha, L. Grandi, Y. Guardincerri and T. Wester, *Model Independent Approach to the Single Photoelectron Calibration of Photomultiplier Tubes*, *Nucl. Instrum. Meth.* **A863** (2017) 35, [[1602.03150](#)].
- [28] A. Manalaysay et al., *Spatially uniform calibration of a liquid xenon detector at low energies using  $^{83\text{m}}\text{Kr}$* , *Rev. Sci. Instrum.* **81** (2010) 073303, [[0908.0616](#)].
- [29] L. W. Kastens, S. Bedikian, S. B. Cahn, A. Manzur and D. N. McKinsey, *A  $^{83\text{Kr}}$  Source for Use in Low-background Liquid Xenon Time Projection Chambers*, *JINST* **5** (2010) P05006, [[0912.2337](#)].
- [30] S. Bruenner et al., *Radon daughter removal from PTFE surfaces and its application in liquid xenon detectors, in preparation* (expected 2020) .
- [31] J. F. Ziegler, M. D. Ziegler and J. P. Biersack, *SRIM - The stopping and range of ions in matter* (2010), *Nucl. Instrum. Meth.* **B268** (2010) 1818.
- [32] L. M. P. Fernandes et al., *Primary and secondary scintillation measurements in a xenon gas proportional scintillation counter*, *JINST* **5** (2010) P09006.

- [33] XENON collaboration, E. Aprile et al., *Signal Yields of keV Electronic Recoils and Their Discrimination from Nuclear Recoils in Liquid Xenon*, *Phys. Rev.* **D97** (2018) 092007, [[1709.10149](#)].
- [34] XENON collaboration, E. Aprile et al., *Intrinsic backgrounds from Rn and Kr in the XENON100 experiment*, *Eur. Phys. J. C* **C78** (2018) 132, [[1708.03617](#)].
- [35] GEANT4 collaboration, S. Agostinelli et al., *GEANT4: A Simulation toolkit*, *Nucl. Instrum. Meth. A* **506** (2003) 250–303.
- [36] B. Karlsson and C. G. Ribbing, *Optical constants and spectral selectivity of stainless steel and its oxides*, *J. Appl. Phys.* **53** (1982) 6340–6346.
- [37] S. Bricola et al., *Noble-gas liquid detectors: measurement of light diffusion and reflectivity on commonly adopted inner surface materials*, *Nucl. Phys. B Proc. Suppl.* **172** (2007) 260 – 262.
- [38] S. Kravitz, R. Smith, L. Hagaman, E. Bernard, D. McKinsey, L. Rudd et al., *Measurements of Angle-Resolved Reflectivity of PTFE in Liquid Xenon with IBEX*, *Eur. Phys. J. C* **80** (2020) 262, [[1909.08730](#)].
- [39] P. Kubelka and F. Munk, *Ein Beitrag zur Optik der Farbanstriche*, *Zeitschrift für technische Physik* **12** (1931) 593–601.
- [40] P. Kubelka, *New Contributions to the Optics of Intensely Light-Scattering Materials. Part I*, *J. Opt. Soc. Am.* **38** (May, 1948) 448–457.
- [41] L. Althueser, S. Lindemann, M. Murra, M. Schumann, C. Wittweg and C. Weinheimer, *VUV Transmission of PTFE for Xenon-based Particle Detectors*, [[2006.05827v1](#)].
- [42] DARWIN collaboration, J. Aalbers et al., *DARWIN: Towards the Ultimate Dark Matter Detector*, *JCAP* **1611** (2016) 017, [[1606.07001](#)].